

The Cranked Nilsson-Strutinsky versus the Spherical Shell Model: A Comparative Study of pf -Shell Nuclei

Andrius Juodagalvis^{1,2)}, Ingemar Ragnarsson¹⁾, and Sven Åberg¹⁾

¹⁾*Mathematical Physics, Lund Institute of Technology*

P.O. Box 118, S-221 00 Lund, Sweden and

²⁾*GSI, Planckstr. 1, 64291 Darmstadt, Germany*

(Dated: November 3, 2018)

A comparative study is performed of a deformed mean field theory, represented by the cranked Nilsson-Strutinsky (CNS) model, and the spherical shell model. Energy spectra, occupation numbers, $B(E2)$ -values, and spectroscopic quadrupole moments in the light pf shell nuclei are calculated in the two models and compared. The result is also compared to available experimental data which are generally well described by the shell model. Although the Nilsson-Strutinsky calculation does not include pairing, both the subshell occupation numbers and quadrupole properties are found to be rather similar in the two models. It is also shown that “unpaired” shell model calculations produce very similar energies as the CNS at all spins. The role of the pairing energy in the description of backbending and signature splitting in odd-mass nuclei is also discussed.

PACS numbers: 21.10.G; 21.10.Ky; 21.60.C; 21.60.Cs; 21.60.Ev; 23.20.-g; 27.40.+z

Keywords: Nuclear structure; shell model; collective model; cranked Nilsson-Strutinsky; calculated electromagnetic moments and transitions; occupation numbers; nuclear deformation; triaxiality; yrast states; signature splitting; isoscalar and isovector pairing energies; pf -shell nuclei

I. INTRODUCTION

A large number of models have been developed to get insight into the spectroscopic properties of nuclei. Two of the most successful models are the spherical shell model and the deformed shell model. Large-scale spherical shell model calculations provide excellent agreement with observed data, but less transparent physics interpretations. The deformed shell model, on the other hand, is a mean field approach that is more illustrative but gives a less accurate agreement with data. A parallel study using the two models allows a better understanding of the underlying nuclear processes. In this paper we aim at comparing the predictions of the spherical shell model (SM) and one version of the deformed shell model, namely, the configuration-dependent cranked Nilsson-Strutinsky (CNS) approach.

For nuclei in the mass region $A \sim 40$ -50 with valence particles occupying pf -shell orbits, well-tested shell model calculations are available [1]. Nuclei in this region show several interesting collective phenomena, such as the existence of rotational bands, backbending of the yrast band, band termination, and the appearance of superdeformed as well as axially asymmetric shapes (triaxiality) [2, 3, 4]. Other interesting features which have been discussed for these nuclei are the role of isoscalar and isovector pairing [1, 5], violation of SU(3) symmetry [6, 7], violation of isospin symmetry [8, 9], angular momentum dependence of the mirror energy difference [8, 10, 11, 12, 13, 14], and Jacobi shapes [15]. This long, by no means complete list indicates the significant attention that these nuclei received in the last few years.

Though both the spherical shell model and the cranked Nilsson-Strutinsky model provide a microscopic description of a nucleus, they are basically different. One dif-

ference is that the shell model gives a laboratory frame description, while the CNS provides a description in the intrinsic frame of reference. Another difference is the ‘model space’ and the treatment of the nuclear interaction. Within the restricted model space of the spherical shell model, the residual interaction between the valence particles is completely taken into account. The deformed shell model uses a virtually unrestricted model space. However, only specific parts of the nuclear interaction are included, in particular the quadrupole-quadrupole interaction. Furthermore, the inclusion of this interaction is made in the mean-field approximation, with the self-consistency condition treated in an approximate way through the Strutinsky energy theorem [16]. Comparison of the two models allows to identify the missing parts of the nuclear interaction as well as correlations beyond the mean field in the deformed shell model on one hand, and the model space limitations in the spherical shell model on the other hand.

The development of the shell model computer code ANTOINE [17] led to extensive and rather systematic theoretical investigations of nuclear spectroscopy in the lower part of pf shell [18, 19, 20, 21] and inspired much experimental work. The (unpaired) cranked Nilsson-Strutinsky model [22, 23] has been applied to more or less all nuclei in the periodic table for which high-spin states have been studied. The model successfully describes terminating rotational bands [22], superdeformed bands [24, 25, 26] and the phenomenon of shape coexistence [27]. This model has also been used to describe a few nuclei in the region of the present study. The interpretation of selected high-spin data in $^{47,48,49}\text{Cr}$ and ^{47}V was discussed in Refs. [22, 28], while the odd-odd nuclei ^{46}V and ^{50}Mn were investigated in Ref. [29].

The spherical shell model was previously compared to the CNS model for some nuclei in the $A \approx 40$ region

[28, 29, 30], and a striking similarity in the predictions was found. In this paper we enlarge the scope of comparison between the two types of models to more nuclei and discuss even-even as well as odd- A nuclei. Backbending, the role of pairing, and in particular its contribution to the signature splitting are stressed. We shall concentrate on the pf -shell nuclei close to the $N = Z$ line with mass numbers between $A = 44$ and 49. By making a more systematic comparison of the two models, we want to improve our understanding of the deformed mean field model, test its validity for fairly light nuclei, and, in particular, to get a better understanding of the physical picture behind the observed properties in the region. This allows to assess the reliability of the CNS approach in heavier nuclei, where spherical shell model calculations are not feasible at present.

The paper is organized in the following way. First, we describe the models in section II. Predictions of the two models are confronted and compared in section III. The paper is summarized in section IV.

II. MODELS

A. The shell model and the cranked Nilsson-Strutinsky model

Shell model results are calculated using the computer code ANTOINE [17]. Valence particles, occupying orbits in the full pf shell, interact via the residual interaction KB3 [31]. For quadrupole properties, effective charges $e_p = 1.5e$, $e_n = 0.5e$ are used. Most of the results obtained with a “full” interaction have already appeared in the publications by the Madrid-Strasbourg group (for a recent review see Ref. [1]). Here we will also present “unpaired calculations” which, with exception of the nucleus ^{48}Cr [32], have not been presented before.

CNS calculations are performed utilizing the modified oscillator potential and a standard set of parameters [22, 23]. The implementation allows to minimize the energy for a fixed configuration at a given value of the total angular momentum with configurations defined as explained in Refs. [22, 33]. The total energy is minimized varying three degrees of freedom: two quadrupole parameters, ε (deformation) and γ (non-axiality), and one hexadecapole parameter, ε_4 [23]. All kinds of pairing interactions are neglected in the CNS approach. Therefore, the CNS results are mainly valid at high spin, and it becomes natural to normalize experimental and calculated energies at some high spin value. This is contrary to the spherical shell model where the corresponding normalization is generally done at the ground state.

The calculated energies are often plotted with a subtracted rotational reference $E_{\text{ref}} = 32.32A^{-5/3}I(I+1)$ MeV [22] in order to facilitate reading of figures and to highlight differences relative to this rotational behavior. The reference corresponds to the rotation-energy of a rigid rotor for a prolate nucleus with a radius constant

$r_0 = 1.20$ fm and a deformation $\varepsilon \approx 0.23$.

B. Moments

A translation between the intrinsic frame of reference and the laboratory frame of reference can be obtained using the rotor model, where those two frames can be related, see [34]. Thus, having values of the quadrupole deformation parameters, ε and γ , it is possible to estimate the strength of the $E2$ transition between two states, $B(E2)$, and the spectroscopic quadrupole moment of a state, Q_{spec} . And vice versa, using the values of $B(E2)$ and Q_{spec} , the quadrupole deformation of a nucleus can be derived. Formally, this identification is valid only for fixed axially symmetric shapes.

In the CNS approach, we calculate the intrinsic quadrupole moments from proton single-particle wave functions at appropriate equilibrium deformations. Neutrons have no contribution to this moment. Since the rotor model assumes axially symmetric shape, while the calculated triaxiality parameter is usually sizeable, we use an approximate relation between the intrinsic moments and laboratory-frame observables [28]. If a nucleus has a rather flat energy surface, quantum fluctuations may become important. To show their effect, in a few selected cases we utilize an approximate method [28] to add the effect of quantum fluctuations on calculated quadrupole properties.

C. Occupation numbers

Single j -shell occupation numbers are readily obtained from the shell model wave-function. In the CNS calculations, the eigenstates are expanded in a stretched basis. It is however straightforward to make a transformation into a spherical basis and then to add up the fractions of the spherical subshells of the eigenstates at the equilibrium deformations. The method is outlined in Ref. [35].

D. Pairing

The shell model includes all kinds of correlations, an important part of which is pairing. To investigate the effect of the pairing interaction, two calculations are performed: one using the full interaction, and another one using the interaction with the pairing force subtracted. As defined in Ref. [32], the pairing energy is the difference between the energies obtained in those two calculations. We consider both the isoscalar (np ; $J = 1$, $T = 0$) and the isovector ($nn+pp+np$; $J = 0$, $T = 1$) $L = 0$ pairing [32, 36]. Thus three kinds of pairing energy are discussed: $T = 0$ pairing energy, which is deduced from the interaction with a subtracted $T = 0$ pairing force; $T = 1$ pairing

energy, which is deduced from the interaction with a subtracted $T = 1$ pairing force; and the full pairing energy, which is deduced from the interaction with both pairing forces subtracted. The strengths of the forces are [36]: $G_{T=0} = -0.51\hbar\omega$ and $G_{T=1} = -0.32\hbar\omega$, where $\hbar\omega = 40A^{-1/3}$ MeV. Since the CNS approach does not include the pairing interaction, it is reasonable to compare its predictions to the “unpaired” energies of the shell model.

III. RESULTS

We compare the two models for the even-even systems in subsection III A, where the nuclei $^{44,46}_{22}\text{Ti}$ and $^{48}_{24}\text{Cr}$ are discussed. For ^{48}Cr , the negative-parity band is discussed in addition to the ground-state band. A few selected odd-even nuclei (namely, $^{45}_{22}\text{Ti}$, $^{47}_{23}\text{V}$ and $^{49}_{24}\text{Cr}$) are discussed in subsection III B.

A. Even-even nuclei

1. Positive-parity band in ^{48}Cr

The nucleus ^{48}Cr has a half-filled $f_{7/2}$ shell of protons and neutrons, resulting in the largest ground-state deformation in the $f_{7/2}$ region. The yrast band shows an interesting behavior, being rotor-like with a backbend and a well-established termination at $I = 16^+$. It has been interpreted as having a triaxial shape [28, 37]. The pairing energy along the band as well as quadrupole properties have been studied extensively [7, 18, 32, 37, 38, 39, 40, 41]. It is, therefore, a good example to start this broader comparison between the CNS and the shell model.

An exploratory study of ^{48}Cr using the CNS and the shell model approaches [28] suggested that the predicted quadrupole properties are similar, although energies are rather different, see Fig. 1. (A similar conclusion was reached when using the cranked Hartree-Fock-Bogolyubov method [6].) We continue this comparison particularly emphasizing the role of the pairing interaction. As in previous studies, we concentrate on the yrast positive-parity, even-spin states between $I = 0$ and 16.

Since pairing is neglected in the CNS calculation, Fig. 1 also shows energies of two “unpaired” shell model calculations. The change in the excitation energies suggests that the backbending behavior is mainly caused by the $T = 1$ pairing (as pointed out in [32] and further discussed in [39]), while the $T = 0$ pairing is generally smaller and decreases smoothly with spin. When the CNS energies are normalized to match the excitation energy of a fully aligned state at $I = 16^+$, they fall between the two unpaired shell model energies; with only the $T = 1$ pairing neglected and all pairing neglected completely, respectively. However, they come much closer to the shell model results without the $T = 1$ pairing. A similar behavior was

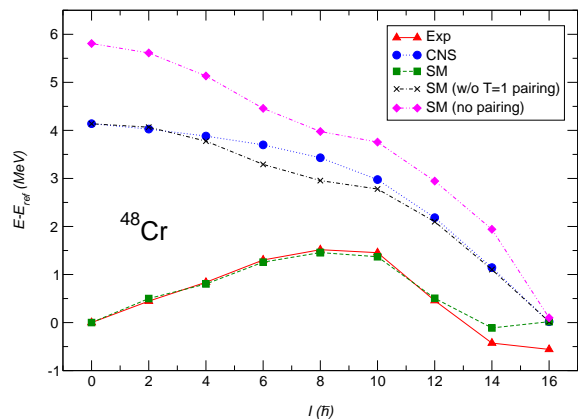


FIG. 1: (Color online) Energies in the ^{48}Cr yrast band plotted relative to a rotational reference. Experimental values [38] are shown by triangles. The other four lines show calculated results: CNS (circles), full shell model (squares), and two “unpaired” shell model cases: without the $T = 1$ pairing (crosses) and without both $T = 0$ and $T = 1$ pairings (diamonds). The calculated CNS energies are matched to the excitation energy of the fully aligned 16^+ state.

noted in Ref. [37], where the shell model and CHFB calculations were compared. There it was attributed to the improper treatment of the proton-neutron pairing by the latter mean-field method [6, 37].

We already noted the similarity of the quadrupole properties as described by the two approaches [28] and will discuss them more below. Here we would like to point out that a more detailed investigation of the results shows that the calculated wave functions are similar as well: The spherical j -shells are occupied almost identically, see Fig. 2. In particular, there is a very good agreement in the occupation of the $f_{7/2}$, $p_{3/2}$ and $p_{1/2}$ shells, despite the fact that the two models treat the “model space” in a different manner, and moreover, pairing is completely neglected in the CNS. The effects of the $T = 1$ pairing interaction are visible in the increased occupation of the $f_{5/2}$ shell and the decreased occupation of the $f_{7/2}$ shell. This is easily understood in the BCS picture of the $T = 1$ pairing. The pairing causes occupations of the orbitals around the Fermi surface to be smeared out, and in ^{48}Cr the Fermi surface is in the middle of the $f_{7/2}$ shell and below the other shells.

The CNS predicts a much lower occupation of the $f_{5/2}$ shell than the shell model (0.06 particles in the ground state as compared to 0.56 particles predicted by the shell model). In addition, some occupation is found outside of the pf shell. The contents of excitations beyond the spherical shell model space decreases smoothly with spin from 0.28 particles in the ground state to zero in the band-terminating state. This agreement in occupation numbers between the two models is remarkable, since

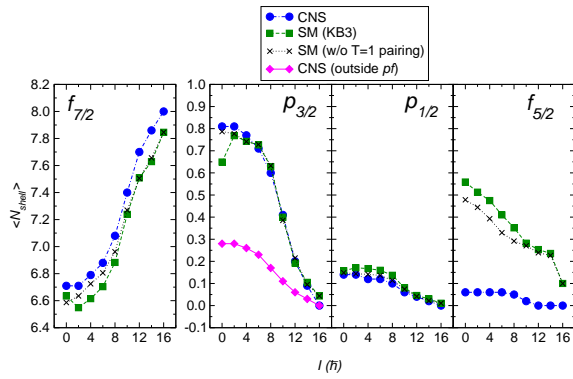


FIG. 2: (Color online) Average number of particles (neutrons and protons) in the spherical j -shells in ^{48}Cr : the shell model values calculated using the full interaction and the interaction without the $T = 1$ pairing are shown by squares and crosses, respectively. The CNS occupancies of the pf shell model orbitals are shown by circles, while the occupancies of orbitals outside the shell model space are shown by diamonds in the panel with the $p_{3/2}$ shell occupancies.

partial occupancies of the spherical j -shells have different origin in the two models. The two-body interaction between valence particles causes configuration mixing in the shell model. On the other hand, the mixing of spherical j -shells is determined by the deformation and rotation in the CNS approach.

Equilibrium deformations calculated in the CNS model at different spin values are shown in Fig. 3. The quadrupole deformation of the ground state, $\epsilon \approx 0.23$, implies a fairly large mixing of the $f_{7/2}$ and $p_{3/2}$ shells, see the Nilsson diagram in Fig. 4. Since all four positive m -states of the $f_{7/2}$ subshell are occupied for protons as well as for neutrons in the band-terminating state 16^+ (cf. Fig. 2), the nucleus obtains a spherical shape. A gradual change in deformation, as the spin increases from 0^+ in the ground state to the 16^+ state (Fig. 3), explains the main changes in the occupation numbers of the $f_{7/2}$ and $p_{3/2}$ shells, seen in Fig. 2. When the deformation decreases, the j -shells get less mixed.

2. Negative-parity band in ^{48}Cr

A negative-parity band in the pf shell nuclei can be obtained by exciting one particle (a proton or a neutron) from a $d_{3/2}$ orbit to an unoccupied $f_{7/2}$ orbit, forming a configuration $d_{3/2}^{-1}f_{7/2}^9$. Denoting the signature quantum number by α , we can write the even-spin configurations (with $\alpha_{\text{tot}} = 0$) as $[\alpha(d_{3/2}^{-1}), \alpha(f_{7/2}^{\text{odd}})] = [-1/2, 1/2]$ and $[1/2, -1/2]$, while the odd-spin configurations (with $\alpha_{\text{tot}} = 1$) are $[-1/2, -1/2]$ and $[1/2, 1/2]$. In the CNS calculations, the odd-spin band with $K^\pi = 4^-$ (excitation

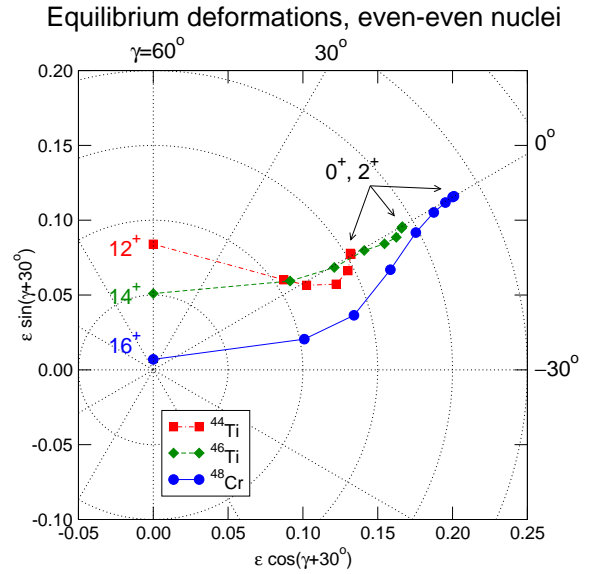


FIG. 3: (Color online) CNS calculated equilibrium deformations along the yrast bands in three even-even nuclei: ^{44}Ti (squares), ^{46}Ti (diamonds) and ^{48}Cr (circles). The deformation change between the $I = 0$ and $I = 2$ states is negligible in all these nuclei.

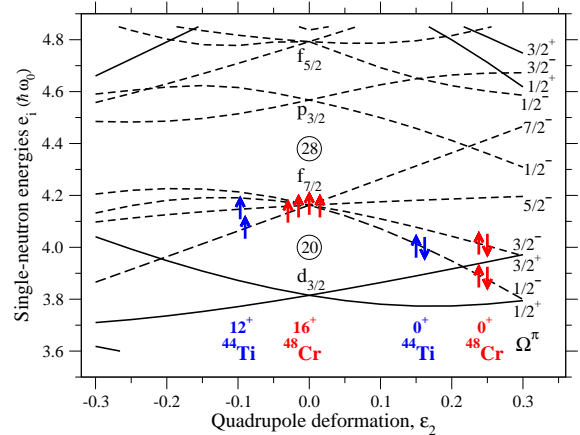


FIG. 4: (Color online) A Nilsson diagram for single-neutron states in the modified oscillator potential. The arrows symbolize particles, while their direction indicates whether m_j is positive (arrow up) or negative (arrow down). The ground state as well as the band-terminating state with all particles in the $f_{7/2}$ shell are shown for ^{48}Cr and ^{44}Ti .

$d_{3/2,3/2}^{-1}f_{5/2,5/2}$) is clearly energetically favored. Other configurations have higher energies. The two bands with $\alpha_{\text{tot}} = 0$ have similar energy values but their equilibrium deformations are somewhat different.

Measured and calculated energies of the negative-parity band in ^{48}Cr are shown in Fig. 5. The measured negative-parity band starts with a 4^- state at $E_x = 3.53$

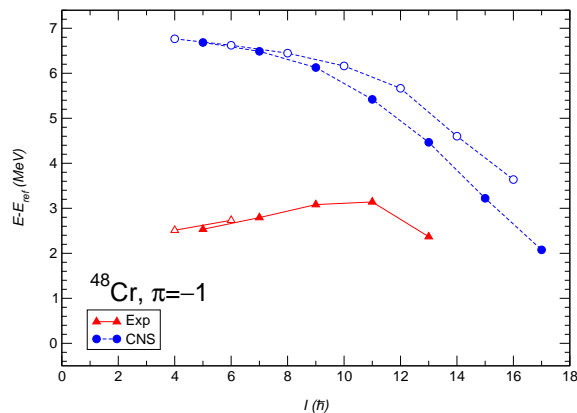


FIG. 5: (Color online) Energies of the negative-parity band in ^{48}Cr : experimental data [38] are shown using triangles, and the CNS results are shown using circles. Filled and empty symbols are used to differentiate between the $\alpha = 1$ and $\alpha = 0$ bands. The CNS energies are normalized in the same way as the ground-state band in Fig. 1.

MeV [2, 42]. Unpaired CNS calculation gives the excitation energy of this state $E_x(4^-) = 3.65$ MeV, which is unexpectedly close to the experimental value. To calculate the unnatural parity bands within the shell model, the model space must be expanded to include at least the $d_{3/2}$ shell. This larger model space calculation is outside of the scope of our paper. We refer to Ref. [38] where such a calculation was reported. Assuming the excitation of a $d_{3/2}$ nucleon to the pf shell, the lower part of the spectrum could be well described, while higher spins were described poorly. These energies are not included in Fig. 5.

Two CNS bands are shown in Fig. 5: the favored configuration with $\alpha_{\text{tot}} = 1$ and one of the $\alpha_{\text{tot}} = 0$ configurations. In both bands the signature of the $d_{3/2}$ hole is $\alpha = -1/2$. The CNS calculation predicts a somewhat bigger moment of inertia than observed experimentally. This can be related to the absence of pairing correlations in the model. If we assume that the spin dependence of the pairing energy is similar to that in ^{49}Cr (see Fig. 16), an approximate prediction of the unobserved energies in the negative-parity band may be obtained (not shown in the figure). In particular, the contribution from the pairing correlations is expected to approximately double the signature splitting predicted by the CNS calculations shown in Fig. 5.

The calculated equilibrium deformations for the negative-parity bands are shown in Fig. 6. The 4^- bandhead has a similar deformation as the 0^+ ground state, in agreement with the measured $B(E2)$ values [38, 43]. However, already this state has a sizeable value of the triaxiality parameter, γ . The non-axiality gets stronger as spin increases, and the band terminates in a non-

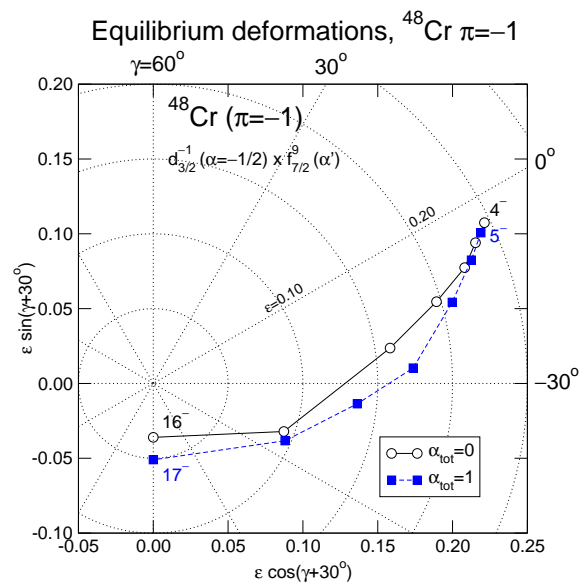


FIG. 6: (Color online) CNS calculated equilibrium deformations in the ^{48}Cr negative-parity band. The odd particle in $f_{7/2}$ has $\alpha' = +1/2$ for the even-spin states ($\alpha_{\text{tot}} = 0$) and $\alpha' = -1/2$ for the odd spins ($\alpha_{\text{tot}} = 1$).

collective prolate shape, having $\gamma = -120^\circ$. In fact, this negative-parity band in ^{48}Cr exhibits the largest calculated negative- γ deformation in the region of pf shell nuclei. This can be understood from Fig. 11 below, where we present the relevant single-particle routhians. A hole in the $N = 2$, $\alpha = +1/2$ orbital, shown in the figure by a solid line, will have a strong polarization effect towards negative- γ values. The excited particle will occupy the 25th or 26th orbital, which are both essentially γ -independent. Thus, the net effect is a large negative- γ deformation of the bands. Since at high spins the spectroscopic quadrupole moment is proportional to $\sin(\gamma + 30^\circ)$ [44], we expect it to be small in this band. The stretched $B(E2)$ values are not much affected by this kind of triaxiality (i.e., by negative γ). Thus a decrease in collectivity towards the band-terminating state is expected.

3. The nuclei ^{44}Ti and ^{46}Ti

Calculated and experimental energies of the yrast states in ^{44}Ti and ^{46}Ti are compared in Fig. 7. These two nuclei have several measured bands, see Refs. [45] and [46] respectively, but we restrict ourselves to the yrast bands only. As expected from the neglect of pairing, the CNS energies deviate from experimental data at low spins. It might appear surprising that the agreement between the shell model results and experiment is not outstanding for ^{44}Ti . However, it is not unexpected, since the pf -shell

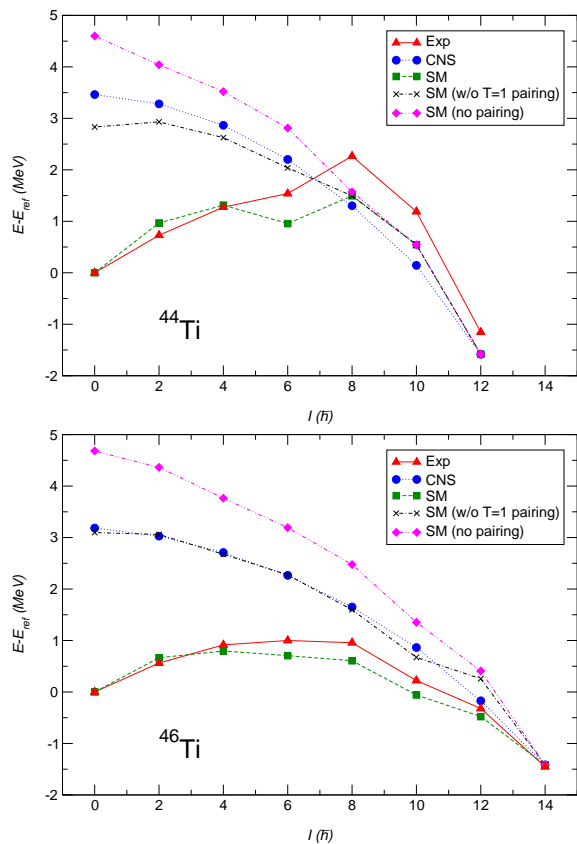


FIG. 7: (Color online) Excitation energies of the yrast states in ^{44}Ti and ^{46}Ti plotted relative to a rotational reference. The experimental energies in ^{44}Ti and ^{46}Ti are taken from Refs. [45] and [46], respectively.

model space is rather restricted for this small number of particles, and the excitations out of the sd shell play an important role in this nucleus [45].

As we already discussed in connection with ^{48}Cr , it is more relevant to compare the CNS energies with the shell model results obtained when the pairing force is removed from the interaction. Therefore Fig. 7 shows two additional lines: the calculated energies when the $T = 1$ pairing is subtracted, and when both the $T = 1$ and $T = 0$ pairings are subtracted. Pairing does not contribute much to the energy for the states above $I = 6$. This is particularly true for ^{44}Ti , where both the $T = 0$ and $T = 1$ pairing energy contributions are approximately zero at $I > 6$. The CNS energies compare well with those unpaired calculations, especially with the one where only the $T = 1$ pairing is removed. Furthermore, the $T = 1$ pairing is the main cause for backbending at $I \approx 10$ in both nuclei, since the $T = 0$ pairing has a smooth dependence, decreasing with spin. All these features are similar to those previously discussed for ^{48}Cr , see Fig. 1.

Having half-filled $f_{7/2}$ shells for both protons and neu-

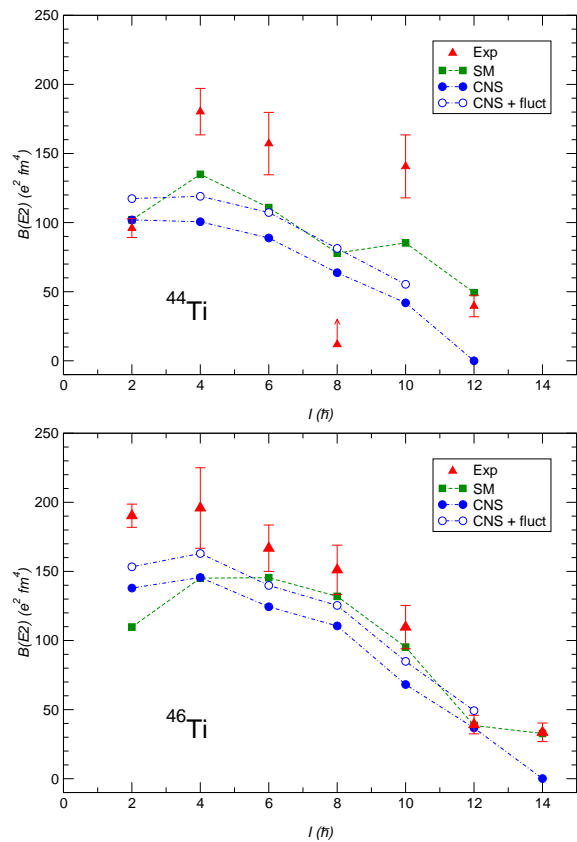


FIG. 8: (Color online) The strength of the stretched $E2$ transitions along the yrast bands of ^{44}Ti and ^{46}Ti . Measured values are taken from Refs. [47, 48] and [3], respectively.

trons, the nucleus ^{48}Cr is the most collective nucleus in the region. By removing one pair of protons from ^{48}Cr we arrive at the nucleus ^{46}Ti . If also a pair of neutrons is removed, we get ^{44}Ti . The quadrupole deformations $\varepsilon=0.15$, 0.19 and 0.23 are predicted for the ground states of the nuclei ^{44}Ti , ^{46}Ti , and ^{48}Cr , respectively, as illustrated in Fig. 3. The origin of this deformation increase with the number of valence particles can be understood by analyzing the Nilsson diagram, see Fig. 4. The lower $f_{7/2}$ orbitals are deformation-driving, thus a gradual increase in the collectivity is expected with the increasing number of valence particles. This was indeed observed in the decays of the 2^+ states to the ground states via $E2$ transitions. The $B(E2)$ values in these three nuclei are: 96 [47], 190 [3], and $311 e^2 \text{fm}^4$ [43]. With 4, 6 and 8 valence particles in the $f_{7/2}$ shell, the rotational bands in ^{44}Ti , ^{46}Ti and ^{48}Cr terminate at $I=12^+$, 14^+ and 16^+ , respectively.

Available experimental information and the calculated $B(E2)$ values for the two titanium isotopes are shown in Fig. 8. The measured values in ^{44}Ti are taken from Ref. [48]. The lifetimes of two levels, 2^+ and 4^+ , were remea-

sured recently by Schielke *et al* [47]. Using the formula $\tau_{1/2} = \log_e(2)/(1.22 \times 10^9 E_\gamma^5 B(E2))$, from the values of 3.97(28)ps and 0.65(6)ps we deduce the $B(E2)$ strengths $96.0 \pm 6.8 e^2 \text{fm}^4$ and $180.3 \pm 16.8 e^2 \text{fm}^4$, respectively. Experimental information on ^{46}Ti is taken from Ref. [3].

Both the shell model and the CNS model suggest a decrease in collectivity as the angular momentum increases in ^{46}Ti and ^{44}Ti , in a similar way as was found in ^{48}Cr [28]. It is astonishing that the transition strengths are so similar in the two models, especially if the CNS results are corrected for quantum fluctuations around the equilibrium, as was described in Ref. [28]. The yrast bands terminate at $I = 12^+$ and 14^+ with some remaining collectivity: According to experiment, the $E2$ transitions from these states have $B(E2)$ values of the order of 4 W.u.

B. Odd-even nuclei

In this subsection we discuss odd-even mass nuclei with $N = Z \pm 1$. In particular, we shall focus on the signature splitting of the yrast band. In subsection III B 1 we present results for the nuclei with the mass $A = 45$ and 47, while results for ^{49}Cr are presented in subsection III B 2. The role of pairing for the backbending as well as signature splitting is discussed in subsection III B 3.

1. $A=45$ and $A=47$ nuclei

The mirror nuclei, $^{45}_{22}\text{Ti}_{23} \text{--} ^{45}_{23}\text{V}_{22}$ and $^{47}_{24}\text{Cr}_{23} \text{--} ^{47}_{23}\text{V}_{24}$, have identical spectra in the shell model description if the Coulomb and other isospin-nonconserving interactions are neglected in favor of a good isospin. In CNS, where protons and neutrons have different single-particle spectra due to the Coulomb interaction, the predicted properties of mirror nuclei are still very similar, since the effect of the Coulomb force (and other isospin-violating interactions) is relatively small in this mass region, i.e. the experimental mirror energy difference is below 100 keV [8, 9, 10]. Because of this similarity in spectra, we present the calculated results only for ^{45}Ti and ^{47}V . Similarly, like in the case of even-even nuclei, we restrict our discussion to the yrast bands.

Experimental and calculated energies of the yrast states in ^{45}Ti and ^{47}V are compared in Fig. 9. In general, the shell model calculations describe the measured energies well. Experimental values are taken from Refs. [49] and [50], respectively. The $\alpha = +1/2$ levels in ^{45}Ti are only known up to $I^\pi = 17/2^-$, and the energy of the $17/2^-$ level in ^{47}V is unknown. In the mirror ^{47}Cr nucleus, the $17/2^-$ level was measured at 3.77 MeV [51]. These missing levels inhibit a discussion of the pair-alignment process in the backbending region, since the mirror energy difference cannot be extracted.

The ground states of ^{45}Ti and ^{47}V are described in the CNS with an odd neutron and proton, occupying

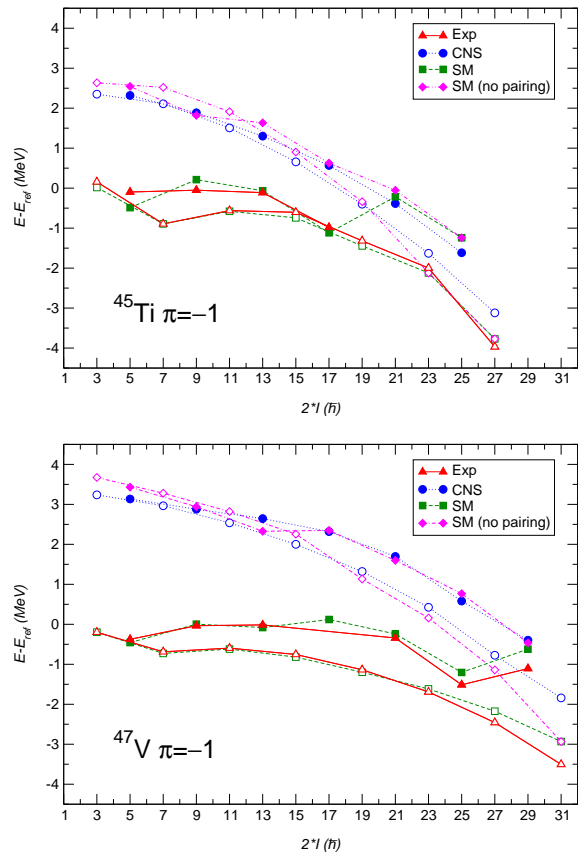


FIG. 9: (Color online) Energies of yrast states in ^{45}Ti and ^{47}V . Experimental data is taken from Refs. [49] and [50], respectively. The levels $21/2^-$ and $25/2^-$ in ^{45}Ti , and the $17/2^-$ state in ^{47}V are not known. Open and empty symbols are used to distinguish the signature $\alpha = +1/2$ and $\alpha = -1/2$ bands.

the $\Omega = 3/2$ state of the $f_{7/2}$ shell, see Fig. 4. This gives rise to a fairly large rotation-induced calculated signature splitting which varies smoothly with spin. The different character of the signature partners, observed experimentally in both nuclei, is thus expected to originate from the pairing force. This conclusion is supported by a remarkably good agreement between the unpaired shell model and the CNS energies, see Fig. 9. Not only the moment of inertia comes out correct but also the signature splitting is fairly well described. Since a similar behavior is also seen in ^{49}Cr (as we will present in the next subsection), we discuss the role of pairing for the signature splitting in subsection III B 3.

Calculated equilibrium deformations for the two signature-partner bands in ^{45}Ti and ^{47}V are shown in Fig. 10. An interesting staggering of the shape is seen. The $\alpha = +1/2$ band has positive γ values, while its signature-partner, $\alpha = -1/2$ band has negative γ values. The different γ -deformations of the two signature bands should mainly affect the quadrupole properties,

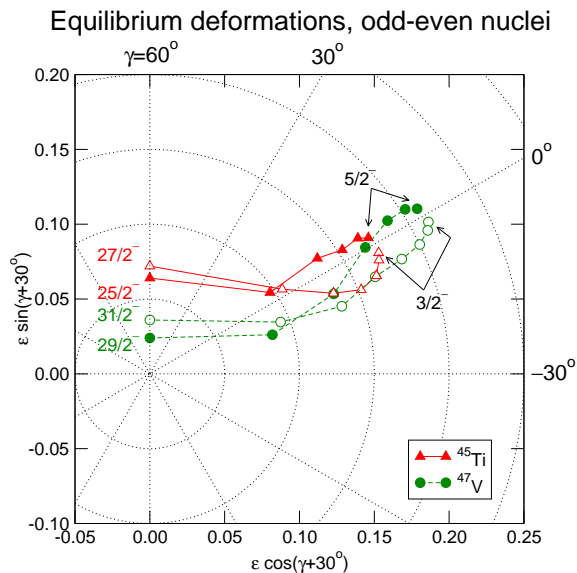


FIG. 10: (Color online) Equilibrium deformations along the yrast band in odd-even nuclei ^{45}Ti (^{45}V) and ^{47}V (^{47}Cr) calculated in the CNS.

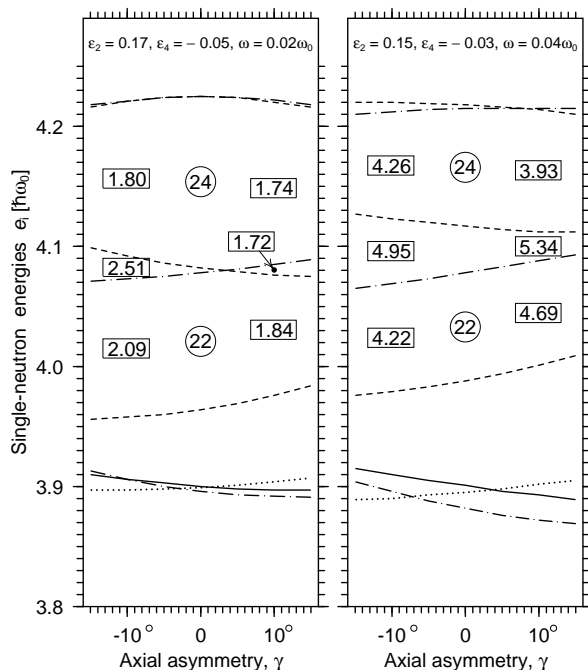


FIG. 11: Dependence of the single-particle routhians on the non-axiality parameter γ at deformations and rotational frequencies relevant for $I \approx 4$ (left panel) and $I \approx 8$ (right panel) states in ^{45}Ti . The encircled numbers indicate the number of orbitals below that point. The boxed numbers show the spin contributions from all 22, 23, and 24 neutrons at $\gamma \pm 10^\circ$. Positive-parity orbitals from the sd ($N = 2$) shell are drawn by full ($\alpha = +1/2$) and dotted ($\alpha = -1/2$) lines. Other lines are negative-parity pf -shell orbitals: $\alpha = +1/2$ orbitals are drawn with dashed lines, while $\alpha = -1/2$ orbitals are drawn with dash-dotted lines. The diagram is drawn for neutrons but the proton orbitals have very similar properties.

while energies are less sensitive to the small changes of the triaxiality parameter. The equilibrium deformations change smoothly from $\varepsilon = 0.17$ (0.21) in the ground state of ^{45}Ti (^{47}V) to $\varepsilon \approx 0.07$ (0.03) in the band-terminating state, having non-collective oblate shape ($\gamma = 60^\circ$). The values of γ parameter do not exceed 10° for most of the states prior to termination.

This different γ -preference may be understood from the single-particle routhians plotted at fixed rotational frequencies in Fig. 11. The encircled numbers show the number of particles below that point. One can clearly see that the 23rd single-particle orbital prefers either a positive or negative γ value, depending on whether the $\alpha = +1/2$ or $-1/2$ branch is occupied. This single-particle orbital is crucial for both $^{45}\text{Ti}_{23}$ and $^{47}\text{Cr}_{23}$, because neither the 22 protons in ^{45}Ti nor the 24 neutrons in ^{47}V have any strong preference in γ . The weak γ -dependence for particle number 24 is also seen from the fact that the ground band of ^{48}Cr is calculated to be nearly axially deformed at low spin values [28]. Since the single-neutron and single-proton level schemes are very similar, the same arguments apply for the nuclei $^{45}\text{V}_{22}$ and $^{47}\text{V}_{24}$.

The routhians of Fig. 11 can also be used to illustrate the triaxial properties of nuclei with N or Z equal to either 22 or 24. The summed effect of the two lowest $f_{7/2}$ orbitals (dashed and dash-dotted lines below particle number 22 in Fig. 11) gives no strong preference in the γ -direction. The 23rd and 24th orbitals have forces driving into different γ -directions, leading to opposite γ -deformations. Their added-up effect cancels the γ -sign preference for 24 particles. There is also a pretty strong driving force of the highest $N = 2$, $\alpha = +1/2$ orbital, which explains large negative- γ deformations in the 1p-1h bands, as we discussed in the case of ^{48}Cr , see III A 2.

2. The nucleus ^{49}Cr

Calculated and experimental yrast energies for ^{49}Cr are shown in Fig. 12. The observed splitting of the signature partners is small at low spins. However, at the spin value $I = 15/2$ the $\alpha = -1/2$ band suddenly changes its smooth behavior in a backbending. The other signature band depends on angular momentum in a smoother way up to the band termination at $31/2^-$. This behavior of the two signature-partner bands is well reproduced in the shell model calculations [20], although there is a systematic deviation at higher spins. The CNS calculations show large deviations, particularly for low spins, as is expected due to the lack of pairing correlations in this model. From the Nilsson diagram (Fig. 4) one can see that in the ground-state configuration the odd neutron occupies the $\Omega=5/2$ orbital of the $f_{7/2}$ shell. This large Ω value causes a rather small signature splitting in the CNS calculation. Similarly as in the case of ^{45}Ti and ^{47}V , the shell model signature splitting reduces if the pairing interaction is removed. These values agree very well with

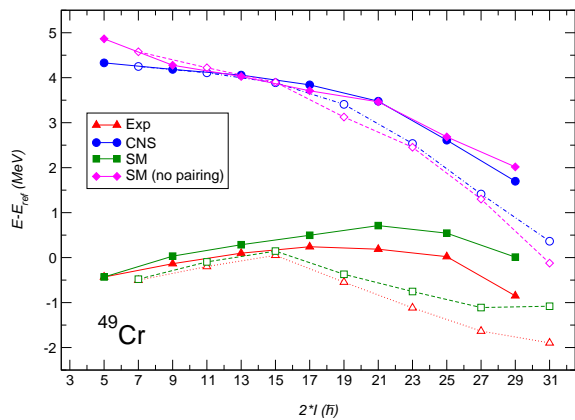


FIG. 12: (Color online) Experimental [50] and calculated energies of yrast states in ^{49}Cr . In addition to the CNS and the shell model calculations (circles and squares, respectively), shell model energies without pairing are shown (diamonds).

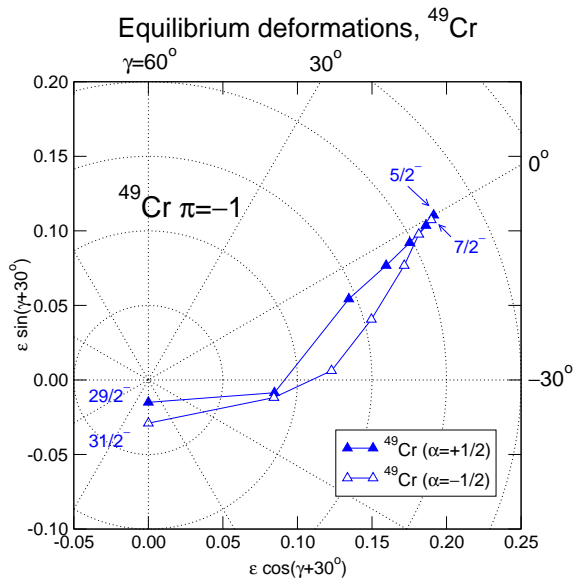


FIG. 13: (Color online) The CNS predicted equilibrium deformations along the yrast band in ^{49}Cr .

the CNS calculation. We explore this observation in a greater detail in the next subsection.

Calculated equilibrium deformations in the lowest $\alpha = +1/2$ and $-1/2$ bands in ^{49}Cr are shown in Fig. 13. The spin dependence of the quadrupole deformation parameter ε was briefly discussed in Ref. [13]. Here we present a more detailed study. Both signature bands prefer negative γ values already at low spins. They terminate in non-collective states with $\gamma = -120^\circ$ at spins $I^\pi = 29/2^-$ and $31/2^-$, respectively. This value of the asymmetry parameter corresponds to a prolate nucleus with the angular momentum aligned along the symmetry axis.

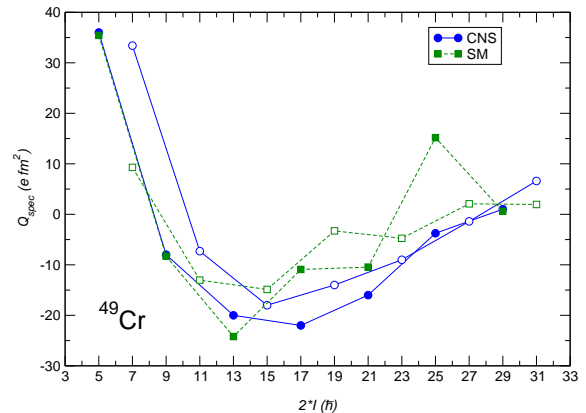
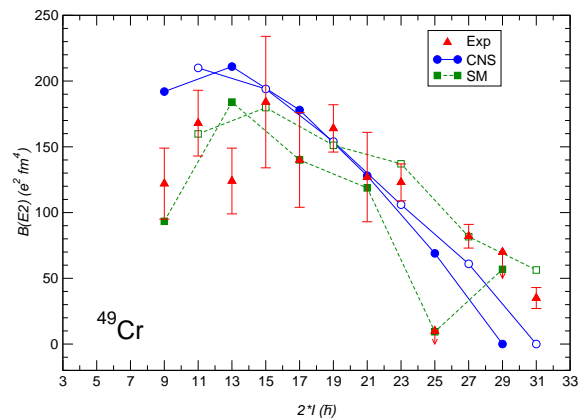


FIG. 14: (Color online) Quadrupole properties of yrast states in ^{49}Cr . The experimental $B(E2)$ values are taken from Ref. [50].

Based on the equilibrium deformations, $B(E2)$ values and spectroscopic moments Q_{spec} were calculated. They are shown in Fig. 14 together with experimental data on $B(E2)$ [50] and the shell model results. (No experimental information on spectroscopic quadrupole moments is available.) The agreement between the two model predictions is remarkable. As seen in Fig. 13, the nuclear shape gradually changes along the band from axially-symmetric prolate to triaxial shapes with negative γ values. Simultaneously, the quadrupole parameter ε gets smaller, which explains the gradual decrease of the $B(E2)$ values for both signatures. It is interesting to note that the quadrupole properties along the signature bands are the same, although the energies in one of them shows a backbending behavior.

As discussed above, the shapes of both signatures in ^{49}Cr change with increasing spin and become clearly triaxial after spin $I > 17/2$, where the rotation takes place around the intermediate axis (negative value of γ in the Lund convention). A signature of nuclear triaxiality in an odd-mass nucleus is the staggering of $B(E2, \Delta I = 1)$ values, as discussed by Hamamoto and Mottelson [44].

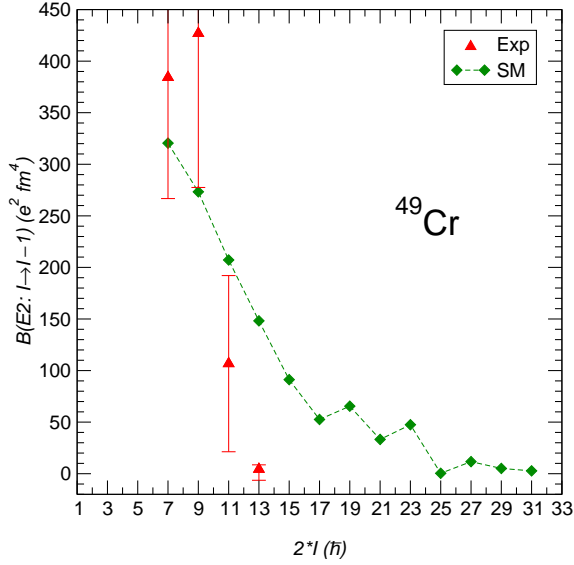


FIG. 15: (Color online) Unstretched $B(E2)$ values in ^{49}Cr : experimental data [52] and the shell model predictions [50]. The staggering occurring at higher spins indicates non-axiality of the nuclear shape [44].

Thus, we plotted them [50, 52] in Fig. 15. It is clearly seen that the staggering in the shell model values of $B(E2; \Delta I = 1)$ indeed appears above the angular momentum $I = 17/2$, when the shapes calculated in CNS become triaxial (Fig. 13).

3. Pairing, Backbending and Signature Splitting

The pairing energy calculated in the shell model has been extensively used above. Subtracting this energy from the shell model value, an unpaired shell model energy could be obtained. Remarkably, this agreed very well with the energies calculated within the unpaired CNS model. This leads us to a more detailed study of the shell model pairing energy, its role in causing backbending of the ground-state band, and its contribution to the signature splitting.

In Fig. 16 we show separately the $T = 0$, the $T = 1$ and the sum of both pairing energies as a function of spin for the three odd-even nuclei ^{45}Ti , ^{47}V , and ^{49}Cr . The $T = 0$ pairing energy behaves smoothly in a similar way as it does in the even-even nucleus ^{48}Cr (see Fig. 4 in [32]). Its contribution decreases from 1-2 MeV in the ground state to a small or zero contribution in the spin-aligned state (the highest angular momentum state shown in the figure). The $T = 1$ pairing shows a pronounced odd-even effect, see Fig. 17. The odd nucleon in the three studied odd-even nuclei implies a blocking effect that weakens the isovector pairing energy by about 1 MeV in the ground

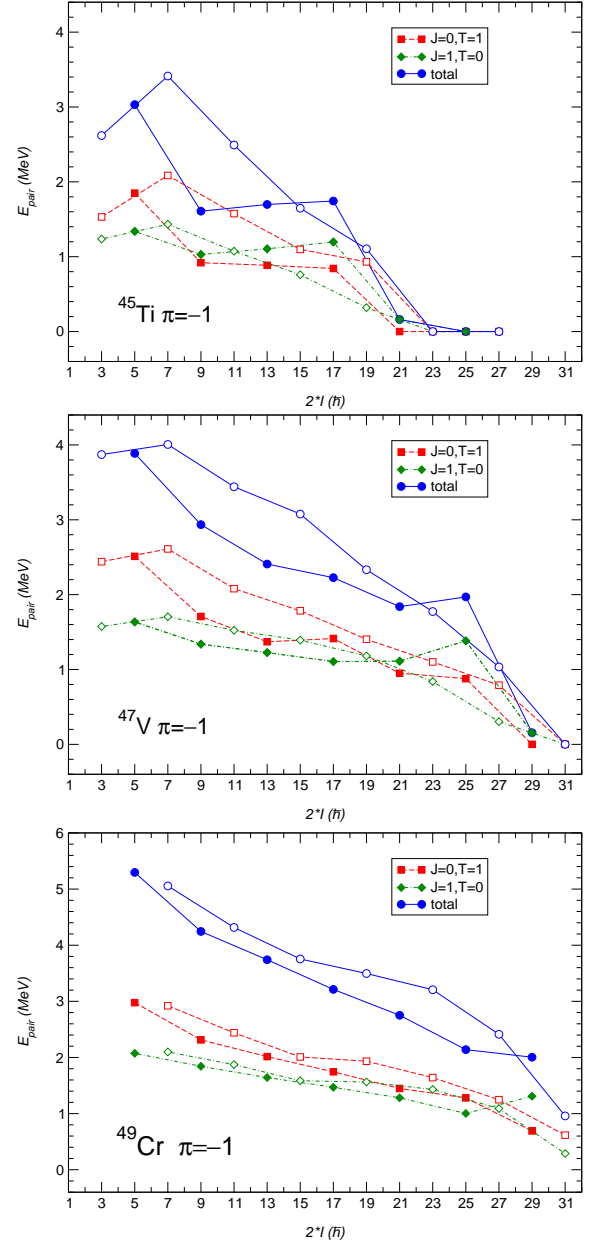


FIG. 16: (Color online) Pairing energy in nuclei ^{45}Ti , ^{47}V , and ^{49}Cr . Filled and open symbols are used to distinguish different signature bands: $\alpha = +1/2$ and $-1/2$, respectively.

state, as compared to the neighboring even-even nuclei. The isoscalar pairing energy has a much smoother mass dependence. Note that the isoscalar pairing contributions seem to follow the same trend along the yrast band as the isovector pairing (Fig. 16). The latter is easy to understand in terms of the seniority. To highlight the change of the $T = 1$ pairing energies, we plot them separately in Fig. 18. One can notice that the increasing

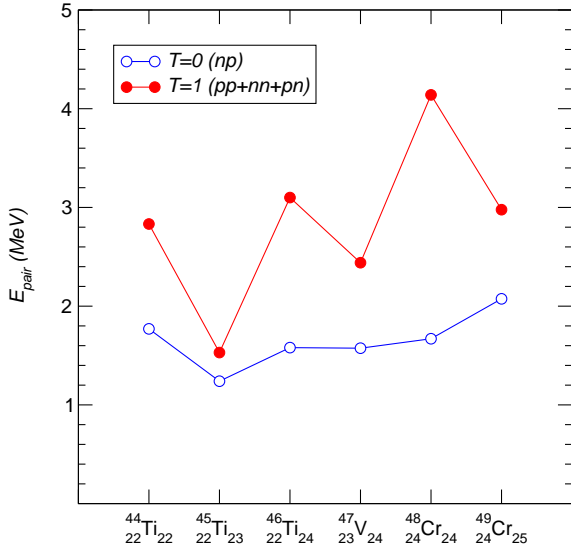


FIG. 17: (Color online) The shell model calculated ground-state pairing energy. The plotted $T = 0$ pairing energy in even-even nuclei is calculated as a difference between the total pairing energy and the $T = 1$ pairing energy.

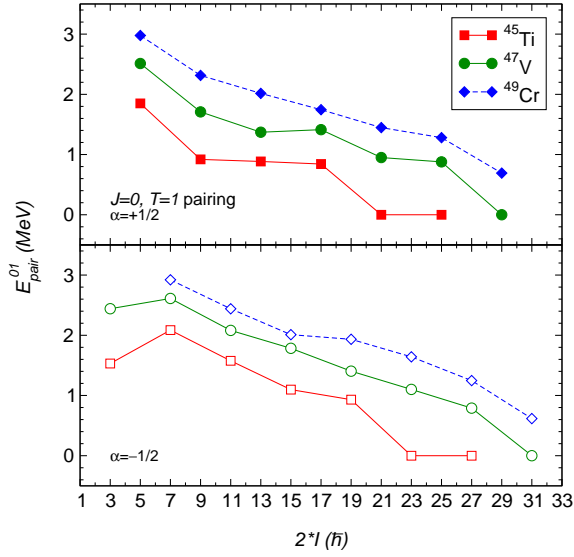


FIG. 18: (Color online) The $J = 0, T = 1$ pairing energy calculated in the shell model for the odd- A nuclei ^{45}Ti , ^{47}V and ^{49}Cr . The upper (lower) panel shows contributions to the $\alpha = +1/2$ ($-1/2$) signature bands.

number of particles increases the collectivity (configuration mixing), and diminishes the irregularities in the spin dependence of the pairing energy.

As we shall see, the changes of the pairing energy with increasing spin causes backbending. Backbending of the yrast band in the nucleus ^{48}Cr has received a great deal of

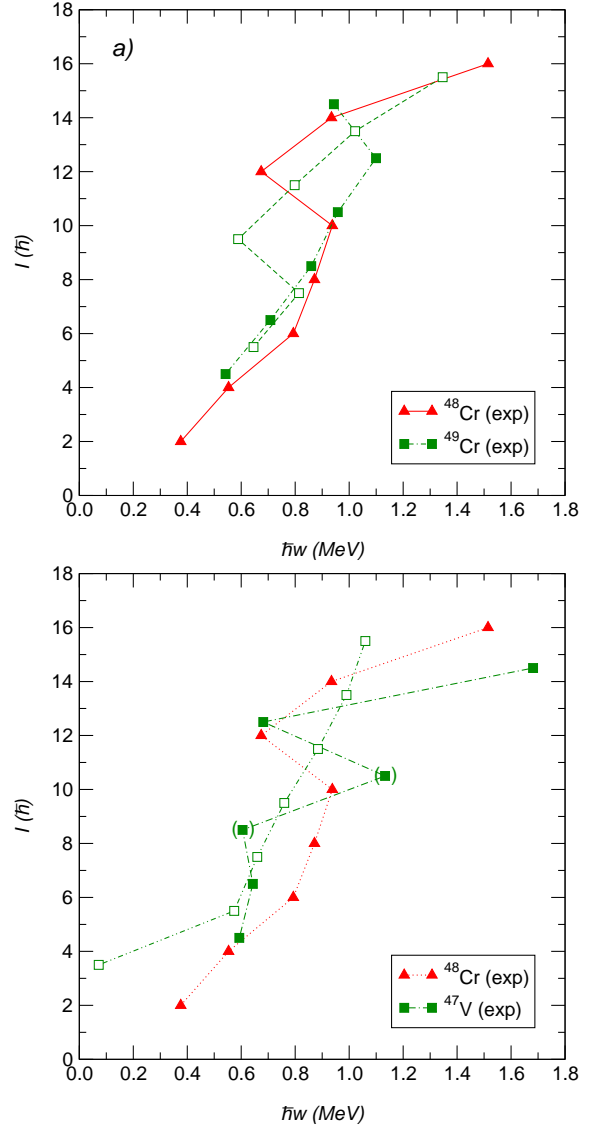


FIG. 19: (Color online) Spin versus rotational frequency in $^{48,49}\text{Cr}$ (top, *a*) and ^{47}V , ^{48}Cr (bottom, *b*). Experimental data are used for Cr isotopes, while for the unknown $17/2^-$ level in ^{47}V , the energy of this level in the mirror nucleus ^{47}Cr is assumed, and the affected transitions are marked by parentheses.

attention, and the usual explanation in terms of a band-crossing is only partly supported by the experimental data. Another important suggestion to explain the observed behavior [3] is the dominance of the seniority $v = 4$ configuration at spin 12^+ [28]. Studies of the spectra of the neighboring nuclei with one proton or neutron either added or removed show energy irregularities along the yrast band. However, it seems to be overseen that this irregularity occurs only in one signature-partner, and not in the other. This is seen from Fig. 19, where we show the

total angular momentum as a function of the rotational frequency $\hbar\omega = [E_\gamma(I) - E_\gamma(I - 2)]/2$. Cameron et al [53] showed the two signatures in ^{49}Cr , but incorrect spin assignments of high-spin states led to a wrong similarity between the bands. Martínez et al [20] stated that the backbending behavior would be seen, if the energies were plotted as spin versus the rotational frequency. However, they did not discuss that in a greater detail nor mention the different behavior of the signature bands.

In a backbending plot, Fig. 19a, we compare the behavior of the two signature bands in ^{49}Cr with the yrast band in ^{48}Cr . The lowest signature band in ^{49}Cr with $\alpha = +1/2$ has a very similar behavior as the yrast band in ^{48}Cr with the difference that the backbend occurs at a lower spin value, $I = 19/2$. The other signature band has a different spin dependence on frequency and exhibits no backbending for spin values $I \approx 10$. The change in the last transition is rather an effect of a band termination [39] than a backbend. A similar difference in the signature partners is also observed in ^{47}V , see Fig. 19b. A difference from ^{49}Cr is that the backbending occurs in the other signature band, $\alpha = +1/2$. Due to the unmeasured $17/2^-$ state in ^{47}V , only the sum of the two transitions $21/2^- \rightarrow 17/2^-$ and $17/2^- \rightarrow 13/2^-$ is known. If, however, we assume that the excitation energy of this state is close to the value measured in the mirror nucleus ^{47}Cr (as we did in the figure), the backbend is clearly seen. Note that independently of the exact value of the $17/2^-$ energy this band will show a backbending.

As we saw in previous subsections, the sum of the $T = 0$ and $T = 1$ pairing energies calculated in the shell model and shown in Fig. 16 seems to describe the missing pairing energy in the CNS calculation for odd- A nuclei quite well, see Figs. 9 and 12. When the pairing energy is subtracted from the shell model energies, no backbending is seen, and the two signature bands behave in a similar way. This implies that pairing causes backbending. Furthermore, pairing increases the signature splitting which is already present because of a rotational coupling. The latter is well described in the CNS model. Further we shall discuss the pairing contribution to the signature splitting that also reveals the different backbending behavior in the two signature bands.

In a simple $f_{7/2}$ shell model for the odd-even nuclei ^{45}Ti , ^{47}V , and ^{49}Cr with only $T = 1$ pairing force considered, the pairing energy in both signature bands is the same. The pairing energy contribution is, however, shifted by 1 unit of angular momentum. For example, the amount of pairing in $5/2^-$ and $7/2^-$ states in ^{49}Cr is the same, because there is no difference in the seniorities of protons and neutrons in these two states: $v_p = 0$, $v_n = 1$. To gain angular momentum, one needs to break pairs, and it is energetically favored to do it in a similar way in both signature partners. Since the $f_{7/2}$ shell is dominant, this similarity is seen in the pairing energy of states with the spins I in the signature $\alpha = +1/2$ band and $(I + 1)$ in the signature partner, see Fig. 18. The curve that describes the pairing energy contribution to

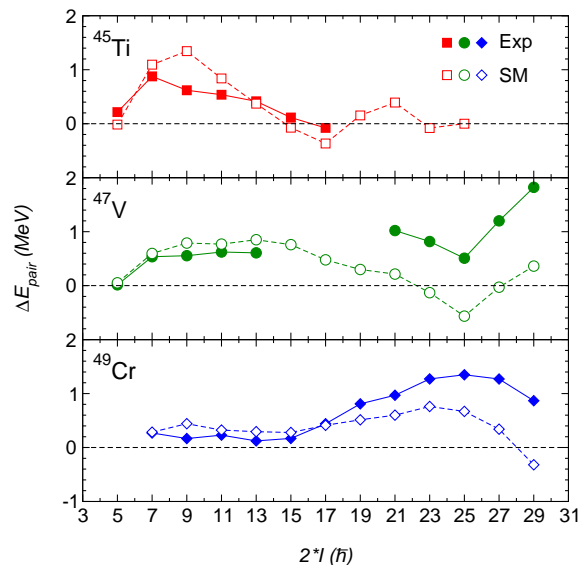


FIG. 20: (Color online) The signature splitting from the total pairing contributions (open symbols) and the experimental values (filled symbols) in ^{45}Ti , ^{47}V and ^{49}Cr .

the $\alpha = -1/2$ band is approximately the same as for the $\alpha = +1/2$ band, but is moved to the right by one unit of angular momentum. This gives a contribution to the signature splitting, since it is defined as the energy difference between the two signature partner bands calculated at a fixed value of angular momentum.

The contribution from $T=0$ and $T=1$ pairing to the signature splitting, ΔE_{pair} , is studied in Fig. 20 for the considered odd-even nuclei. We also show the experimental signature splitting that is seen to follow the trends of the shell model calculation. The difference between the experimental signature splitting and the pairing signature splitting comes from rotational coupling, which is well described in unpaired CNS calculations. The signature splitting from the $T = 0$ pairing behaves smoothly in a similar way as in the even-even nucleus ^{48}Cr (see Fig. 4 in [32]), while the irregular behavior comes from the $T = 1$ part. This can be explained to some extent by a trivial shift by one unit of angular momentum between the two signature partners, as was discussed above. The change of slope of ΔE_{pair} around $I = 25/2$ seen in ^{47}V and around $I = 17/2$ in ^{49}Cr causes the radically different rotational behavior observed for these nuclei, namely that one signature band shows a backbending and the other does not.

IV. SUMMARY AND CONCLUSIONS

A comparison was made between the unpaired cranked Nilsson-Strutinsky model and the spherical shell model.

It was found that quadrupole properties predicted by the two models agree well. Furthermore, the moment of inertia given by the CNS is close to that from the shell model when either only the $T = 1$ pairing is removed (even-even nuclei) or both $T = 1$ and $T = 0$ pairings are removed (odd-even nuclei).

In general, the shell model gives an excellent description of observed signature splittings. It was found that the pairing interaction gives a strong contribution to this splitting. Furthermore, the different spin dependence of the pairing energy for the signature partners in ^{47}V and ^{49}Cr explains why backbending is observed in one but not in the other signature. This behavior comes mainly from the $T = 1$ pairing but is strengthened by the $T = 0$ pairing.

Equilibrium deformations calculated in the CNS model shows that some nuclei in the region have noticeably non-axial shapes with negative γ -values corresponding to rotation around the intermediate axis. These deformations can be traced back to contributions from specific orbitals. The non-axial deformations are supported by the calculated $B(E2)$ values and spectroscopic quadrupole moments, which agree well with experiment as well as with those predicted by the shell model. For ^{44}Ti and ^{46}Ti the contributions from quantum fluctuations around the equilibrium shape lead to an improved agreement with experimental $B(E2)$ transition strengths.

The negative-parity band in ^{48}Cr was discussed. It has the largest calculated negative γ -values in this region. It was also noted that the $B(E2)$ values predicted by the shell model for the unstretched transitions in ^{49}Cr have the expected staggering behavior as a sign of triaxiality.

From this extended comparative study we conclude, that the CNS model gives an adequate description of the quadrupole nuclear properties as well as the occupation numbers of the spherical j -shells. Furthermore, if the pairing energy calculated from the shell model is added to the unpaired CNS energies, excellent agreement to experimental energies is obtained. It would be most interesting to try to include a pairing force in the CNS model that mimics the pairing energy calculated in the shell model. Such a model, which might be applied to all regions of nuclei, could naturally be tested on the pf -shell nuclei studied here.

Acknowledgments

We would like to thank E. Caurier and F. Nowacki for access to the shell model code ANTOINE [17]. I.R. and S.Å. thank the Swedish Natural Science Research Council (NFR).

-
- [1] E. Caurier, G. Martínez-Pinedo, F. Nowacki, A. Poves, and A.P. Zuker, www.arxiv.org: nuclth-0402046.
- [2] C.A. Ur, *Eur. Phys. J. A* 20, 113 (2004).
- [3] F. Brandolini, *Eur. Phys. J. A* 20, 139 (2004).
- [4] S.M. Lenzi, *Nucl. Phys. A* 704, 124c (2002).
- [5] W. Satuła and R. Wyss, *Phys. Rev. Lett.* 87, 052504 (2001).
- [6] A. Poves, *Nucl. Phys. A* 731, 339 (2004).
A. Poves, *in* Conference proceedings “Selected topics on $N = Z$ nuclei: Pingst2000”, D. Rudolph and M. Hellström, Eds., p. 138, (2000, Lund University).
- [7] V.G. Gueorguiev, J.P. Draayer, and C.W. Johnson, *Phys. Rev. C* 63, 014318 (2000).
- [8] A.P. Zuker, S.M. Lenzi, G. Martínez-Pinedo, and A. Poves, *Phys. Rev. Lett.* 89, 142502 (2002).
- [9] P.E. Garrett, W.E. Ormand, D. Appelbe, R.W. Bauer, J.A. Becker, L.A. Bernstein, J.A. Cameron, M.P. Carpenter, R.V.F. Janssens, C.J. Lister, D. Seweryniak, E. Tavukcu, and D.D. Warner, *Phys. Rev. Lett.* 87, 132502 (2001).
- [10] D. Tonev, P. Petkov, A. Dewald, T. Klug, P. von Brentano, W. Andrejtscheff, S.M. Lenzi, D.R. Napoli, N. Marginean, F. Brandolini, C.A. Ur, M. Axiotis, P.G. Bizzeti, and A. Bizzeti-Sona, *Phys. Rev. C* 65, 034314 (2002).
- [11] C.D. O’Leary, M.A. Bentley, S.M. Lenzi, G. Martínez-Pinedo, D.D. Warner, A.M. Bruce, J.A. Cameron, M.P. Carpenter, C.N. Davids, P. Fallon, L. Frankland, W. Gelletly, R.V.F. Janssens, D.T. Joss, C.J. Lister, P.H. Regan, P. Reiter, B. Rubio, D. Seweryniak, C.E. Svensson, S.M. Vincent, and S.J. Williams, *Phys. Lett.* B525, 49 (2002).
- [12] S.M. Lenzi, N. Marginean, D.R. Napoli, C.A. Ur, A.P. Zuker, G. de Angelis, A. Algora, M. Axiotis, D. Bazzacco, N. Belcari, M.A. Bentley, P.G. Bizzeti, A. Bizzeti-Sona, F. Brandolini, P. von Brentano, D. Bucurescu, J.A. Cameron, C. Chandler, M. De Poli, A. Dewald, H. Eberth, E. Farnea, A. Gadea, J. Garcés-Narro, W. Gelletly, H. Grawe, R. Isocrate, D.T. Joss, C.A. Kalfas, T. Klug, T. Lampman, S. Lunardi, T. Martínez, G. Martínez-Pinedo, R. Menegazzo, J. Nyberg, Zs. Podolyak, A. Poves, R.V. Ribas, C. Rossi Alvarez, B. Rubio, J. Sánchez-Solano, P. Spolaore, T. Steinhardt, O. Thelen, D. Tonev, A. Vitturi, W. von Oertzen, and M. Weiszflog, *Phys. Rev. Lett.* 87, 122501 (2001).
- [13] M.A. Bentley, C.D. O’Leary, A. Poves, G. Martínez-Pinedo, D.E. Appelbe, R.A. Bark, D.M. Cullen, S. Ertürk, and A. Maj, *Phys. Lett.* B437 (1998) 243. Erratum in *Phys. Lett.* B451, 445 (1999).
- [14] M.A. Bentley, C.D. O’Leary, A. Poves, G. Martínez-Pinedo, D.E. Appelbe, R.A. Bark, D.M. Cullen, S. Ertürk, and A. Maj, *J. Part. G* 25, 599 (1999).
- [15] A. Maj, M. Kmiecik, A. Bracco, F. Camera, P. Bednarczyk, B. Herskind, S. Brambilla, G. Benzoni, M. Brekiesz, D. Curien, G. De Angelis, E. Farnea, J. Grębosz, M. Kicińska-Habior, S. Leoni, W. Męczyński, B. Million, D.R. Napoli, J. Nyberg, C.M. Petrache, J. Styczeń, O. Wieland, M. Ziębliński, K. Zuber, N. Dubray, J. Dudek and K. Pomorski, *Nucl. Phys. A* 731, 319 (2004).
- [16] V.M. Strutinsky, *Nucl. Phys. A* 122, 1 (1968).

- [17] E. Caurier, computer code ANTOINE, CRN, Strasbourg, 1989.
- [18] E. Caurier, A.P. Zuker, A. Poves and G. Martínez-Pinedo, Phys. Rev. C 50, 225 (1994).
- [19] G. Martínez-Pinedo, A. Poves, L.M. Robledo, E. Caurier, F. Nowacki, J. Retamosa, A.P. Zuker, Phys. Rev. C 54, R2150 (1996).
- [20] G. Martínez-Pinedo, A.P. Zuker, A. Poves, E. Caurier, Phys. Rev. C 55, 187 (1997).
- [21] C.E. Svensson, S.M. Lenzi, D.R. Napoli, A. Poves, C.A. Ur, D. Bazzacco, F. Brandolini, J.A. Cameron, G. de Angelis, A. Gadea, D.S. Haslip, S. Lunardi, E.E. Maqueda, G. Martínez-Pinedo, M.A. Nagarajan, C. Rossi Alvarez, A. Vitturi, J.C. Waddington, Phys. Rev. C 58, R2621 (1998).
- [22] A.V. Afanasjev, D.B. Fossan, G.J. Lane and I. Ragnarsson, Phys. Rep. 322, 1 (1999).
- [23] T. Bengtsson and I. Ragnarsson, Nucl. Phys. A436, 14 (1985).
- [24] I. Ragnarsson, Nucl. Phys. A557, 167c (1993).
- [25] A.V. Afanasjev and I. Ragnarsson, Nucl. Phys. A608, 176 (1996).
- [26] A.V. Afanasjev, I. Ragnarsson and P. Ring, Phys. Rev. C 59, 3166 (1999).
- [27] W.C. Ma, R.V.F. Janssens, T.L. Khoo, I. Ragnarsson, M.A. Riley, M.P. Carpenter, J.R. Terry, J.P. Zhang, I. Ahmad, P. Bhattacharyya, P.J. Daly, S.M. Fischer, J.H. Hamilton, T. Lauritsen, D.T. Nisius, A.V. Ramayya, R.K. Vadapalli, P.G. Varmette, J.W. Watson, C.T. Zhang, and S.J. Zhu, Phys. Rev. C 65, 034312 (2002).
- [28] A. Juodagalvis, I. Ragnarsson, and S. Åberg, Phys. Lett. B477, 66 (2000).
- [29] B.-G. Dong and H.-Ch. Guo, Eur. Phys. J. A17, 25 (2003).
- [30] C.E. Svensson, A.O. Macchiavelli, A. Juodagalvis, A. Poves, I. Ragnarsson, S. Åberg, D.E. Appelbe, R.A.E. Austin, C. Baktash, G.C. Ball, M.P. Carpenter, E. Caurier, R.M. Clark, M. Cromaz, M.A. Deleplanque, R.M. Diamond, P. Fallon, M. Furlotti, A. Galindo-Urribari, R.V.F. Janssens, G.J. Lane, I.Y. Lee, M. Lipoglavsek, F. Nowacki, S.D. Paul, D.C. Radford, D.G. Sarantites, D. Seweryniak, F.S. Stephens, V. Tomov, K. Vetter, D. Ward, and C.H. Yu, Phys. Rev. Lett. 85, 2693 (2000).
- [31] A. Poves and A.P. Zuker, Phys. Rep. 70, 235 (1981).
- [32] A. Poves and G. Martínez-Pinedo, Phys. Lett. B430, 203 (1998).
- [33] A.V. Afanasjev and I. Ragnarsson, Nucl. Phys. A591, 387 (1995).
- [34] Aa. Bohr and B.R. Mottelson, Nuclear Structure, vol. II (W.A. Benjamin, New York, 1975).
- [35] R.K. Sheline, I. Ragnarsson, S. Åberg, and A. Watt, J. Phys. G: Nucl. Phys. 14, 1201 (1988).
- [36] M. Dufour and A.P. Zuker, Phys. Rev. C 54, 1641 (1996).
- [37] E. Caurier, J.L. Egido, G. Martínez-Pinedo, A. Poves, J. Retamosa, L.M. Robledo, and A.P. Zuker, Phys. Rev. Lett. 75, 2466 (1995).
- [38] F. Brandolini, S.M. Lenzi, D.R. Napoli, R.V. Ribas, H. Somaal, C.A. Ur, D. Bazzacco, J.A. Cameron, G. de Angelis, M. De Poli, C. Fahlander, A. Gadea, S. Lunardi, G. Martínez-Pinedo, N.H. Medina, C. Rossi Alvarez, J. Sánchez-Solano, C.E. Svensson, Nucl. Phys. A642, 387 (1998).
- [39] A. Juodagalvis and S. Åberg, Phys. Lett. B 428, 227 (1998).
- [40] K. Hara, Y. Sun, and T. Mizusaki, Phys. Rev. Lett. 83, 1922 (1999).
- [41] T. Tanaka, K. Iwasawa, and F. Sakata, Phys. Rev. C 58, 2765 (1998).
- [42] S.M. Lenzi, *Contribution to the Symposium on Nuclear Structure Physics with EUROBALL: Achievements 1997-2002, Orsay, 2002*.
- [43] T.W. Burrows, Nucl. Data Sheets 68, 1 (1993).
- [44] I. Hamamoto and B.R. Mottelson, Phys. Lett. B132, 7 (1983).
- [45] C.D. O'Leary, M.A. Bentley, B.A. Brown, D.E. Appelbe, R.A. Bark, D.M. Cullen, S. Ertürk, A. Maj, and A.C. Merchant, Phys. Rev. C 61, 064314 (2000).
- [46] D. Bucurescu, C.A. Ur, S.M. Lenzi, D.R. Napoli, J. Sánchez-Solano, D. Bazzacco, F. Brandolini, G. de Angelis, E. Farnea, A. Gadea, S. Lunardi, N. Mărginean, Zs. Podolyak, A. Poves, and C. Rossi Alvarez, Phys. Rev. C 67, 034306 (2003).
- [47] S. Schielke, K.-H. Speidel, O. Kenn, J. Leske, N. Gemein, M. Offer, Y.Y. Sharon, L. Zamick, J. Gerber, and P. Maier-Komor, Phys. Lett. B567, 153 (2003).
- [48] J.A. Cameron and B. Singh, Nucl. Data Sheets 88, 299 (1999).
- [49] P. Bednarczyk, J. Styczeń, R. Broda, M. Lach, W. Męczyński, D. Bazzacco, F. Brandolini, G. de Angelis, S. Lunardi, L. Müller, N.H. Medina, D.R. Napoli, C.M. Petrache, C. Rossi Alvarez, F. Scarlassara, G.F. Segato, C. Signorini, F. Soramel, Eur. Phys. J A2, 157 (1998).
- [50] F. Brandolini, N.H. Medina, S.M. Lenzi, D.R. Napoli, A. Poves, R.V. Ribas, J. Sanchez-Solano, C.A. Ur, M. De Poli, N. Mărginean, D. Bazzacco, J.A. Cameron, G. de Angelis, A. Gadea, R. Menegazzo, and C. Rossi-Alvarez, Nucl. Phys. A693, 517 (2001).
- [51] J.A. Cameron, M.A. Bentley, A.M. Bruce, R.A. Cunningham, W. Gelletly, H.G. Price, J. Simpson, D.D. Warner, and A.N. James, Phys. Rev. C 49, 1347 (1994).
- [52] T.W. Burrows, Nucl. Data Sheets 76, 191 (1995).
- [53] J.A. Cameron, M.A. Bentley, A.M. Bruce, R.A. Cunningham, W. Gelletly, H.G. Price, J. Simpson, D.D. Warner, and A.N. James, Phys. Lett. B 235, 239 (1990).